8-8-2018

Fingerprinting Sediment Transport in River-Dominated Margins Using Combined Mineral Magnetic and Radionuclide Methods

Jinlong Wang
State Key Laboratory of Estuarine and Coastal Research, East China Normal University, Shanghai, China

Weigou Zhang
State Key Laboratory of Estuarine and Coastal Research, East China Normal University, Shanghai, China

M. Baskaran
Wayne State University, baskaran@wayne.edu

Jinzhou Du
State Key Laboratory of Estuarine and Coastal Research, East China Normal University, Shanghai, China, jzdu@sklec.ecnu.edu.cn

Feng Zhou
State Key Laboratory of Satellite Ocean Environment Dynamics, Second Institute of Oceanography, State Oceanic Administration, Hangzhou, China

See next page for additional authors

Journal of Geophysical Research: Oceans

RESEARCH ARTICLE
10.1029/2018JC014174

Key Points:
- The $^{7}Be/^{210}Pb_{ex}$ and χ_{ARM}/SIRM ratios of surface sediments in the estuary region of the East China Sea varied seasonally
- Both ^{210}Pb budget and SIRM data suggest that only a fraction of particles could be transported out of the inner shelf of the ECS
- A combined analysis of radionuclides and magnetic properties offers a better understanding of sediment transport in river-dominated margins

Supporting Information:
- Supporting Information S1

Correspondence to:
J. Du,
jzdu@sklec.ecnu.edu.cn

Citation:
Wang, J., Zhang, W., Baskaran, M., Du, J., Zhou, F., & Wu, H. (2018). Fingerprinting sediment transport in river-dominated margins using combined mineral magnetic and radionuclide methods. *Journal of Geophysical Research: Oceans*, *123*, 5360–5374. https://doi.org/10.1029/2018JC014174

Received 14 MAY 2018
Accepted 7 JUL 2018
Accepted article online 23 JUL 2018
Published online 8 AUG 2018

Fingerprinting Sediment Transport in River-Dominated Margins Using Combined Mineral Magnetic and Radionuclide Methods

Jinlong Wang[1], Weiguo Zhang[1], Mark Baskaran[2], Jinzhou Du[1], Feng Zhou[3], and Hui Wu[1]

[1]State Key Laboratory of Estuarine and Coastal Research, East China Normal University, Shanghai, China, [2]Department of Geology, Wayne State University, Detroit, MI, USA, [3]State Key Laboratory of Satellite Ocean Environment Dynamics, Second Institute of Oceanography, State Oceanic Administration, Hangzhou, China

Abstract Both magnetic properties and radionuclides are widely used to trace sediment transport in aquatic environments; however, these methods have not been used in combination. In this study, the East China Sea (ECS), a typical river-dominated margin, was chosen to demonstrate the advantages of combining these two methods to track sediment movements on a seasonal to annual timescale. The ratios between saturation isothermal remnant magnetization and anhysteretic remnant magnetization (χ_{ARM}/SIRM) and $^{7}Be/^{210}Pb_{ex}$ activity ratios as well as mass balance of ^{7}Be provide information on the seasonal transport of sediment from the Changjiang Estuary to the neighboring shelf. Both ^{210}Pb budget and SIRM distribution in the inner shelf of the ECS show that a small fraction (at most 14% of annual Changjiang sediment discharge) of particles could be transported offshore. Most of ^{7}Be activities in inner shelf sediments of the ECS were below detection limit due to relatively lower residence times and dilution by the older sediment. The observation that radionuclide activities exhibit a better correlation with χ_{ARM}/SIRM ratios than with grain size suggests that iron oxides are the primary carriers of ^{7}Be, ^{210}Pb, and ^{234}Th. The absorption of radionuclides onto magnetic minerals further reinforces the reliability of this combined approach in tracing sediment transport. Our study indicates that radionuclides, with different half-lives, can be utilized for quantifying sediment dynamics, whereas magnetic properties can yield more detailed information on sediment transport directions. The combined analysis of magnetic parameters and radionuclides offers a better understanding of sediment transport in river-dominated areas.

1. Introduction

In the river-dominated margins that are impacted by land-derived freshwater and/or sediments (Mckee et al., 2004), sediment transport and deposition processes not only affect morphological changes but also play a vital role in the biogeochemical cycle of particulate organic carbon, heavy metals, and organic pollutants (Aller, 1998; Aller et al., 2004; Bianchi, 2011; Giffin & Corbett, 2003). Recently, fluvial sediment input to the river-dominated margins has experienced rapid changes due to human activities and climate change (Syvitski et al., 2009; Wei et al., 2014). Hence, study of sediment dynamics in this environment has received wide attention (Hoitink et al., 2017). Particle-reactive radionuclides that have short half-lives (e.g., ^{7}Be, ^{210}Pb, and ^{234}Th) have been widely utilized to trace the transport of sediments from rivers to oceans (e.g., Allison et al., 2005; Baskaran et al., 1996; Baskaran & Santschi, 2002; Du et al., 2016). These radionuclides adsorb onto particulate matter and thereby can serve as particle tracers, with distribution coefficient (K_d) values of 10^{4}–10^{6} ml/g in estuarine and coastal waters (e.g., Baskaran & Santschi, 1993; Feng et al., 1999). In marine environments, ^{7}Be ($T_{1/2}$: 53.3 days) and ^{210}Pb ($T_{1/2}$: 22.3 years) are primarily derived from atmospheric deposition and riverine input as well as boundary scavenging also affecting their sources to varying extent in different regions (Palinkas et al., 2005; Saari et al., 2010; Smoak et al., 1996), while ^{234}Th ($T_{1/2}$: 24.1 days) is mainly derived from the decay of dissolved ^{238}U in seawater. Because the activities of radionuclides in sediments are influenced by particle size as well as by mineralogy (Singleton et al., 2017), the activity ratios of radionuclides (e.g., $^{7}Be/^{234}Th$ and $^{7}Be/^{210}Pb$) are commonly used in order to normalize the effects of particle size on scavenging (e.g., Feng et al., 1999; Laceby et al., 2017).

The advantage of such radionuclide tracers is that they offer timescales of sediment transport and deposition. Depending on their half-lives, these radionuclides can be used to investigate sediment dynamics on daily,

monthly, annual, and decadal timescales. However, owing to the influence of mineralogy, half-lives, and sources, the utilization of such radionuclides as tracers of sediment movement may yield different results depending on the radionuclides utilized. For example, in a previous study, $^{7}Be/^{210}Pb_{ex}$ activity ratio was not expected to decrease from the Gironde estuary to the ocean during low river discharge because of the primarily oceanic source of dissolved ^{7}Be (Saari et al., 2010). Therefore, the use of radionuclides as tracers of sediment transport requires a detailed examination of the mechanism (e.g., time scales of processes and constraining boundary conditions) and its suitability, although this method has been utilized to determine timescales of modern sedimentation in estuarine and coastal settings based on certain assumptions, such as radionuclides, is irreversibly absorbed onto particles and transported with particles without any desorption or fractionation (Feng et al., 1999; Huang et al., 2013; McKee et al., 1983). Magnetic minerals (mainly iron oxides such as magnetite) are ubiquitous in sediments and are sensitive to their sources of origin and variations in sorting due to particle size, density, and shape along the transport pathway (e.g., Li et al., 2017; Nguyen et al., 2016). Therefore, magnetic minerals have been widely used to trace sediment transport processes in different environmental settings (Evans & Heller, 2003; Hatfield et al., 2010; Kim et al., 2013; Thompson & Oldfield, 1986). Because magnetic measurements are relatively simple and fast, analyses of magnetic properties could be useful in supplementing the radionuclide method in sediment transport studies.

To the best of our knowledge, no studies have yet focused on the combined use of magnetic properties and radionuclides as tracers of sediment transport, although each of these methods has been utilized individually to analyze sediment transport around the world (e.g., Du et al., 2010; Ge et al., 2015; Horng & Huh, 2011; Nguyen et al., 2016; Sommerfield et al., 1999; Wang et al., 2017; Zhang et al., 2012). In this study, we have chosen the East China Sea (ECS), which is a typical river-dominated marginal sea of the Pacific Ocean (Liu et al., 2007; Mckee et al., 2004), as a case study area to demonstrate the advantages of the combined use of radionuclides and magnetic methods. Though a number of studies have discussed the sediment dynamics in the ECS, the cross-shelf transport flux of sedimentary particles to the middle shelf have not been estimated (e.g., Liu et al., 2006; Zhu et al., 2011). It is expected that this combined approach using multitracers offers not only a better understanding of the transport of sedimentary materials in the ECS but also additional insights into sediment transport in other river-dominated areas.

2. Materials and Methods

The ECS (Figure 1), with a total area of 7.7×10^5 km^2, has a broad (approximately 350–640 km width), shallow (mean water depth: 72 m), and flat (mean gradient: 0.037%) continental shelf. The ECS receives abundant terrestrial sediment from the Changjiang (Yangtze River). It is estimated that ~40% of the fluvial sediment is trapped in the estuary, and the remaining 60% is transported to the neighboring continental shelf of the ECS (Liu et al., 2006; Milliman et al., 1985). In recent years, Changjiang has exhibited a decrease in its sediment discharge from 0.43×10^9 ton/year in 2000 to 0.2×10^9 ton/year in 2011 due to construction of impoundments (e.g., Three Gorges Dam) and soil conservation in the catchment (Dai et al., 2014). Near the Changjiang mouth, the inner shelf is mainly composed of silts and clayey silts. To the south of the Changjiang, a mud area that is approximately 800 km long exists parallel to the coast (Liu et al., 2006). The ECS has a complicated current system, which was described by Su (2001); it includes the northward flowing Taiwan Warm Current (TWC) and Kuroshio Current (KC). At the mouth of the Changjiang, the Changjiang Diluted Water (CDW) flows southward in winter but turns northeastward in summer. Along the coast, the Yellow Sea Coastal Current (YSCC) and the Zhejiang-Fujian Coastal Current (ZFCC), which contain high concentrations of suspended particles, are strong in winter and weak in summer. Farther offshore, the Yellow Sea Warm Current (YSWC) flows northward and intersect with the YSCC to form a loop current.

Sampling of surface sediment has been reported in our previous study (Wang et al., 2016). The samples were collected during the R/V *Shiyan 3* cruise in spring, from 15 May to 4 June 2011, as well as during the *Beidou* cruise, from 16 to 26 August 2011 using a box core and subsampled using an acrylic core tube with a diameter of 10 cm. Samples were sealed in plastic bags and stored in a freezer at 4 °C. Sampling depths were dictated by the thickness of yellow colored sediment, which was inferred to be a mobile mud layer based on homogeneous grain size and radionuclide activities (Corbett et al., 2004; Wang et al., 2016). Therefore, sampling thickness was different at each location and varied between ~1 and 5 cm at most stations except a few stations closer to Changjiang Estuary (~10 cm). Original data on the thickness, water content, grain

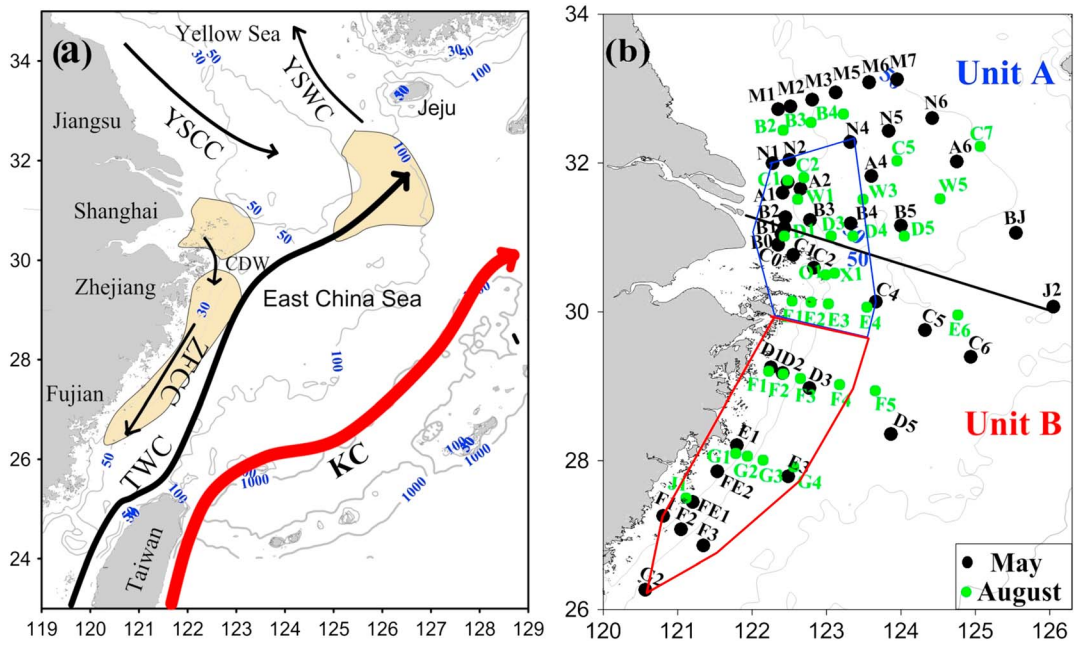

Figure 1. (a) The regional surface currents in spring, modified from Su (2001): Changjiang Dilute Water (CDW); Zhejiang-Fujian Coast Current (ZFCC); Yellow Sea Coastal Current (YSCC); Yellow Sea Warm Current (YSWC); Taiwan Warm Current (TWC); Kuroshio Current (KC). (b) Locations of sampling sites during the spring and summer cruises in 2011. The bathymetry (m) of the ECS shelf is shown as grey lines, and the muddy area is marked by a yellow color (modified after Liu et al., 2006). The black line (b) represents the boundary of the two units (A and B) identified using magnetic properties. The closed areas with blue and red boxes represent the estuary region and inner shelf of the ECS for radionuclides budget estimation, respectively.

size, and activities of radionuclides in these surface sediments and sampling locations were reported in the Table 1 and Table S1 of our previous study (Wang et al., 2016). For magnetic measurements, low-frequency (0.47 kHz) and high-frequency (4.7 kHz) susceptibilities (χ) were measured using a magnetic susceptibility meter (Bartington Instruments MS2B). Anhysteretic remnant magnetization (ARM), which is expressed as χ_{ARM}, was induced in a Dtech 2000 alternating demagnetizer using a peak AF field of 100 mT imposed with a DC biasing field of 0.04 mT. Saturation isothermal remnant magnetization (SIRM) was generated after applying a field of 1 T; then, backfield remanence was obtained at −100 and −300 mT (IRM_{-100} and IRM_{-300}, respectively) using an MMPM10 pulse magnetizer. The remanence was measured using a Molspin Minispin fluxgate magnetometer. The *Hard* IRM (HIRM) is defined as (SIRM + IRM_{-300})/2; S_{-100} and S_{-300} are defined as 0.5 × (SIRM − IRM_{-100})/SIRM and 0.5 × (SIRM − IRM_{-300})/SIRM, respectively (Bloemendal & Liu, 2005; Thompson & Oldfield, 1986).

3. Results and Discussion

3.1. Spatial Distribution of Magnetic Properties

The measured values of magnetic parameters (χ, SIRM, HIRM, χ_{ARM}, S_{-100}, S_{-300}, χ_{ARM}/SIRM, and χ_{ARM}/χ) were listed in Table S1. Values of χ and SIRM generally reflect the concentration of ferrimagnetic minerals (e.g., magnetite) in the sediment, while values of HIRM are measures of the quantities of *hard* magnetic minerals, such as hematite and goethite (Thompson & Oldfield, 1986). The values of χ, SIRM and HIRM of surface sediments collected in May had similar magnitude to those samples collected in August. Generally, the χ, SIRM, and HIRM values showed similar spatial distributions (Figure 2), and they decreased offshore. During May 2011, the maximum χ values were found in the northern region of the study area (Figure 2a), where values were greater than 100×10^{-8} m^3/kg and decreased from west to southeast. Also, this region showed higher χ, SIRM, and HIRM values in May than those in August. Values of χ_{ARM} are sensitive to the grain size of ferrimagnetic mineral, and the χ_{ARM} values of stable single domain grains were higher than those of superparamagnetic grains and multidomain grains (Maher, 1988). The decreasing trend of χ_{ARM} along the

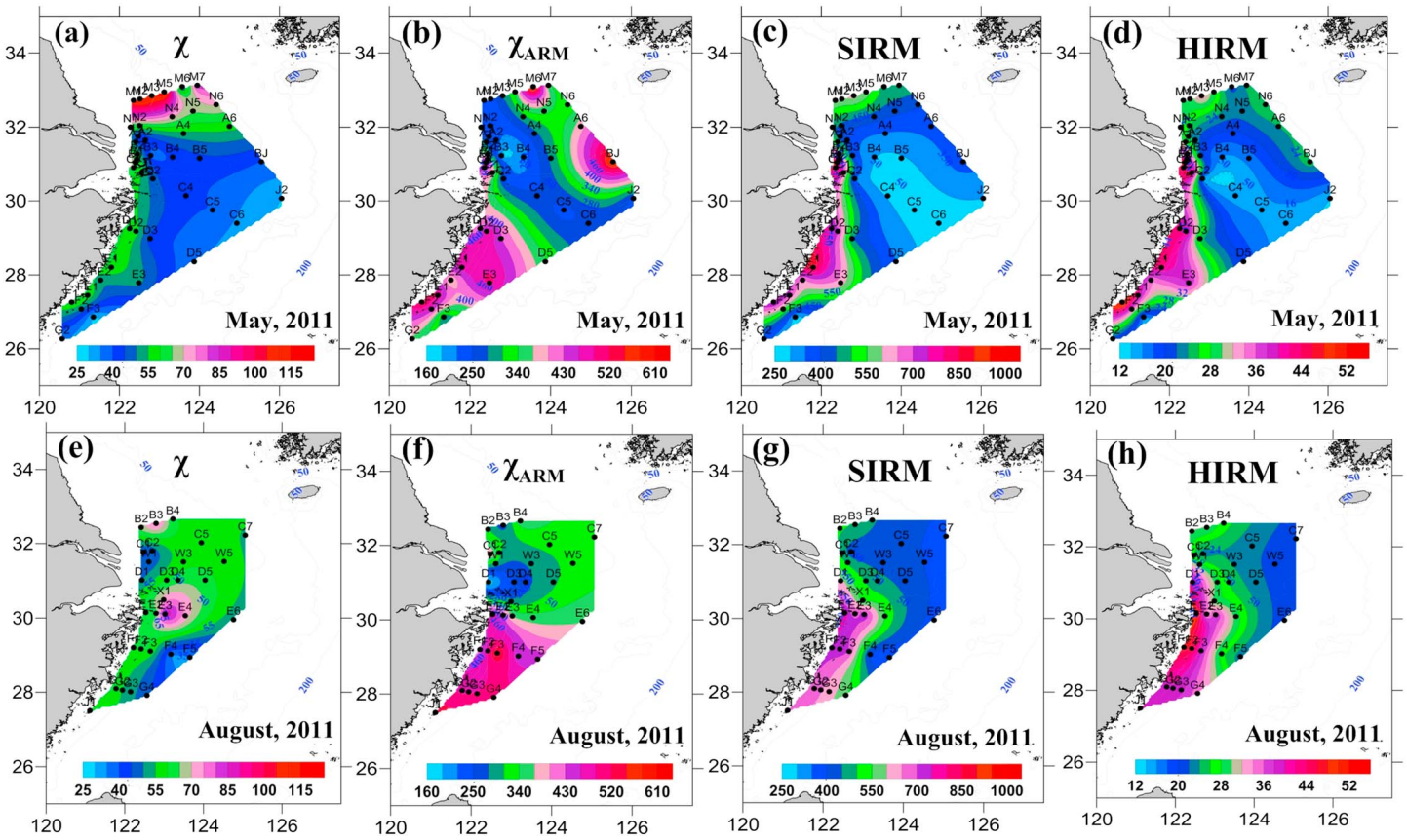

Figure 2. Spatial distribution of χ (10^{-8} m^3/kg), χ_{ARM} (10^{-8} m^3/kg), SIRM (10^{-5} Am^2/kg), and HIRM (10^{-5} Am^2/kg) values of surface sediments in (a–d) May and (e–h) August.

Zhe-Min coast (Figures 2b and 2f) suggested that the single domain size of magnetic minerals decreased offshore. This decrease may be due to the offshore sorting of the sediment, which leads to removal of ferrimagnetic minerals on the transport pathway (Nguyen et al., 2016), as well as the dilution by relict sand with lower χ_{ARM} values in the Zhe-Min coast (Liu et al., 2010).

The values of S_{-100} and S_{-300} can be used to estimate the proportion of low- to high-coercivity magnetic minerals in a sample (Bloemendal & Liu, 2005; Kruiver et al., 2001; Thompson & Oldfield, 1986). The ranges of S_{-300} and S_{-100} values observed in both May and August were not significantly different from each other (Figure 3). These high values of S_{-300} (>90% on average) and S_{-100} (>86% on average) suggest that magnetic properties of these samples were dominated by ferrimagnetic minerals. Generally, the S-ratios, especially S_{-300}, showed relatively little variation (Figure 3), which demonstrated that their magnetic mineralogy assemblages are similar. The ratios of χ_{ARM}/χ and χ_{ARM}/SIRM are indicative of ferrimagnetic mineral grain size, with higher ratios corresponding to finer ferrimagnetic grain sizes (Banerjee et al., 1981; Maher, 1988). The minimum values of the χ_{ARM}/χ ratio were observed in the coastal area, and their maximum values were observed offshore (Figures 3c and 3f).

3.2. Implications of Magnetic Properties for Sediment Transport

Previous studies have shown that magnetic properties of sediments are influenced by sediment source, sorting, and diagenesis (Thompson & Oldfield, 1986). In the river-dominated margin, sediments contain significant fractions of refractory terrestrial organic matter. The terrestrial organic matter can be oxidized through multiple deposition-resuspension cycles, and degradation through iron and sulfate reduction in surface sediments can be weak (Blair & Aller, 2012). Ferrimagnetic minerals, which are only a small portion of iron oxides, dominate magnetic properties of sediments. Reductive dissolution of ferrimagnetic minerals in surface sediment is not so important in the river-dominated margin (Roberts, 2015). The concentration

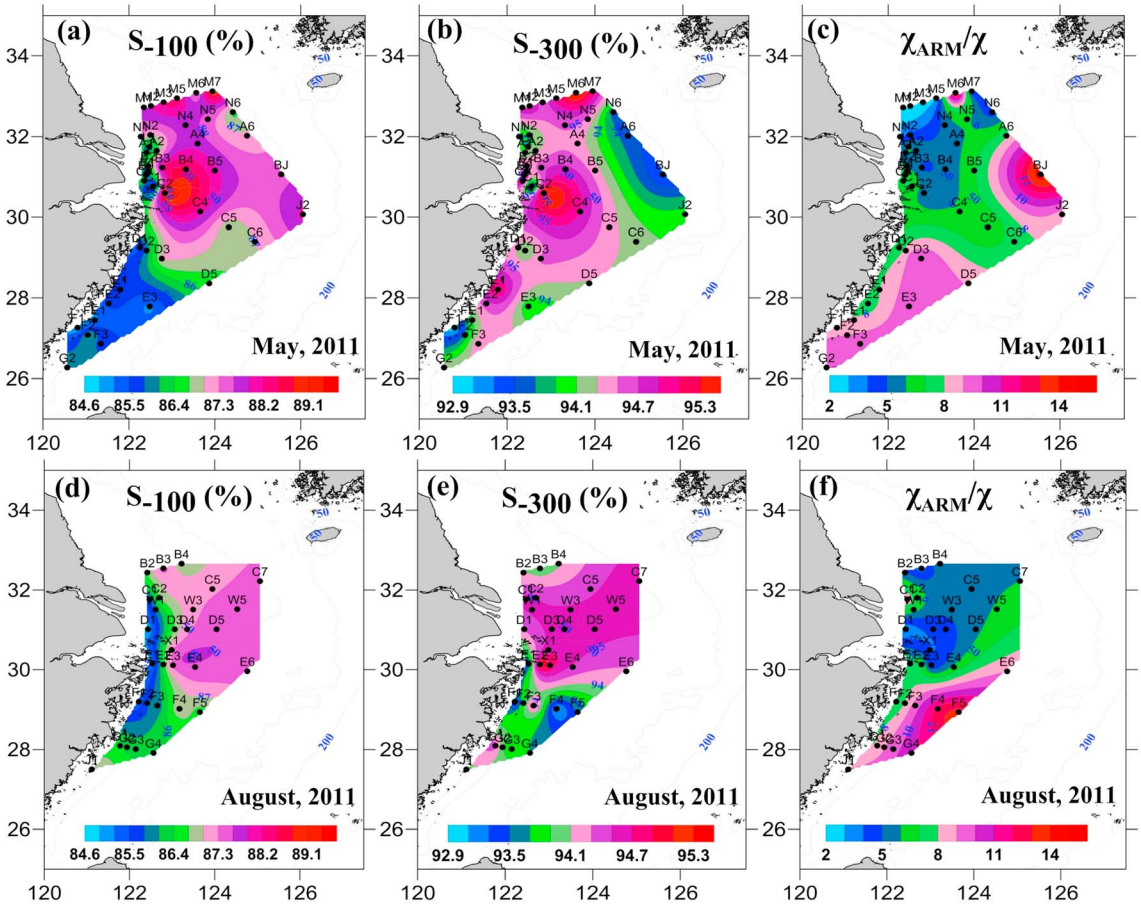

Figure 3. Spatial distribution of S_{-100} (%), S_{-300} (%), and χ_{ARM}/χ values of surface sediments in (a–c) May and (d–f) August.

and magnetic parameters (e.g., χ and SIRM) are stable in the upper several decimeters of sediment cores in the study area with higher sedimentation rate (Ge et al., 2015). Thus, the influences of diagenetic processes on magnetic properties of surface sediments are expected to be minor.

Surface sediments to the south of the Changjiang Estuary include modern Changjiang-derived sediments in the inner shelf (with higher χ and SIRM values), relict sands offshore (with lower χ and SIRM values), and mixed sediments with intermediate values (Liu et al., 2010). In addition, earlier studies have shown that the study area received sediments from the southward delivery of eroded former Yellow River delta (old Huanghe delta; Lin et al., 2002). The plot of χ versus SIRM enabled identification of two groups (Figure 4), which are located in two different regions (Figure 1b). The spatial distribution of Units A and B are primarily related to their different sources of sediments. The χ and SIRM values observed at station B0 are the same as those that have been reported from Changjiang sediment ([73 ± 20] × 10^{-8} m^3/kg and [1,090 ± 250] × 10^{-5} Am^2/kg, respectively; Zhang et al., 2008). The sediments transported to Unit A represent a mixture of Changjiang-derived minerals with continental shelf relict sands (Liu et al., 2010). The sediments in the northern part of the ECS appear to be a mixture of relict sands and materials from the northern Jiangsu coast. A previous study suggested that materials in the northern Jiangsu coast were mainly derived from the old Huanghe delta, where 0.5–1.0 × 10^9 tons/year of sediments were eroded and transported southward (Zhou et al., 2014).

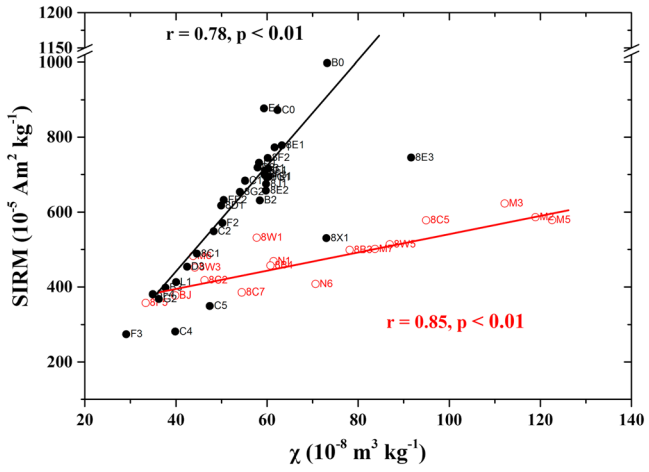

Figure 4. The relationships between χ and SIRM of samples collected from unit A (red circle) and unit B (black dot).

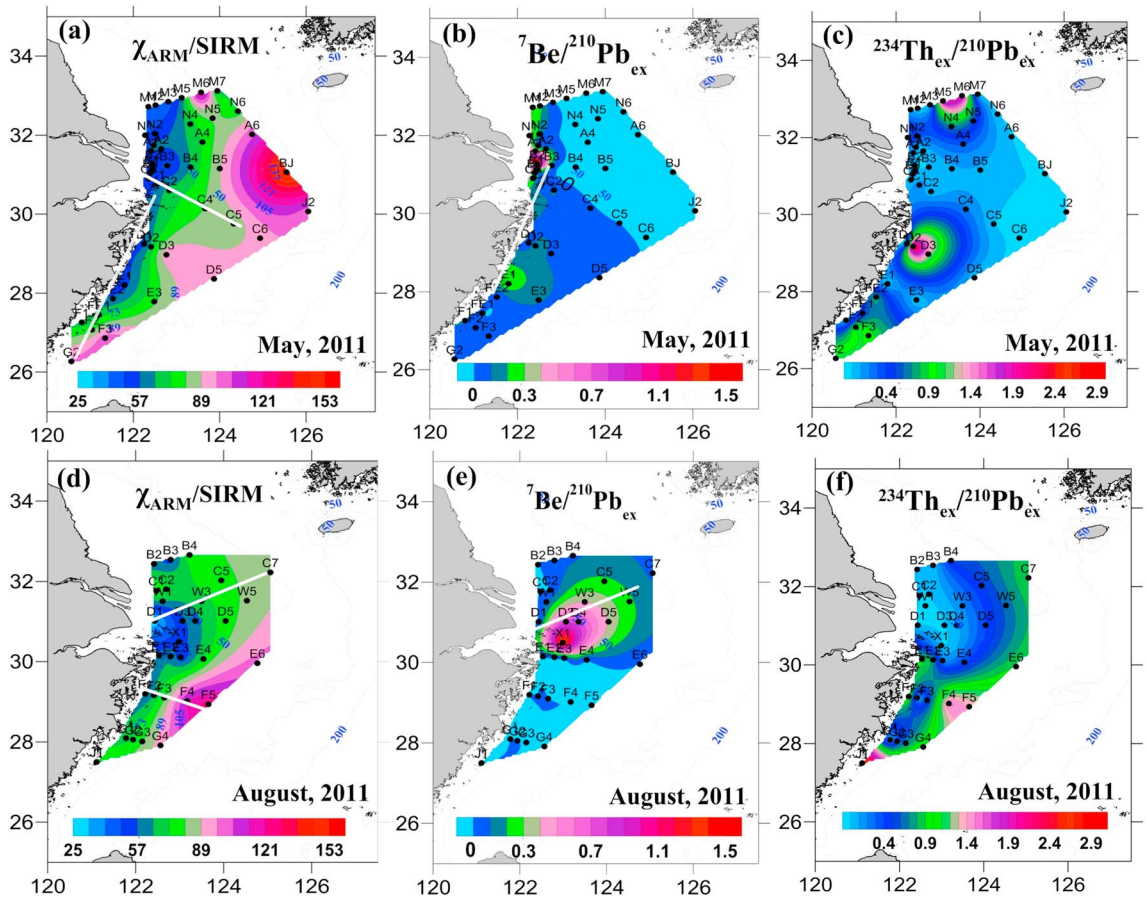

Figure 5. Spatial distribution of χ_{ARM}/SIRM ratios and $^{7}Be/^{210}Pb_{ex}$, $^{234}Th_{ex}/^{210}Pb_{ex}$, activity ratios in (a–c) May and (d–f) August.

It is noted that the maximum χ value was observed at the offshore region of the northern Jiangsu coast (i.e., M2). However, this site has an intermediate SIRM value. Sorting process likely causes higher χ value at this site. The sediments around station M2 were relatively coarser, which was likely due to the frequent occurrence of sedimentary sorting resulting from strong hydrodynamic conditions (Shi & Wang, 2010; Xing et al., 2012). This sorting process could lead to the transport of finer particles farther off the coast, while the coarser and heavier particles that are retained locally contain a larger paramagnetic mineral fraction, which contributes to higher χ value without increasing the SIRM value (Dong et al., 2014).

Among the magnetic parameters, the χ_{ARM}/SIRM ratio has been found to increase with increasing distance from the source on the transport pathway (e.g., Dong et al., 2014; Nguyen et al., 2016). This trend reflects the fact that ferrimagnetic minerals are sensitive to hydrodynamic sorting, as fine-grained particles can be transported farther away than coarse-grained particles. The spatial variation of χ_{ARM}/SIRM ratio varied seasonally near the estuary. It increased from the river mouth toward the south (from L1 to G2) in May (Figure 5a) and toward the northeast (from 8D1 to 8C7) in August (Figure 5d). In addition, the χ_{ARM}/SIRM ratios increased from the coast to offshore during both seasons in the Zhe-Min mud area, thus suggesting offshore transport of sediment. SIRM, χ, and HIRM values also exhibited similar distribution patterns in both seasons, which indicates that the offshore transport of sediment is not influenced by the seasonal reversal of ZFCC. As discussed above, the sources of sediments in the northern region of the ECS included Changjiang input, Yellow Sea input, and relict sand; hence, we could not use the two end-member model to quantify the contribution from each source. However, the sources of sediments in the southern region of the ECS are Chanjiang input and relict sands, and we can use the following equation to estimate their contributions to the magnetic minerals in this region:

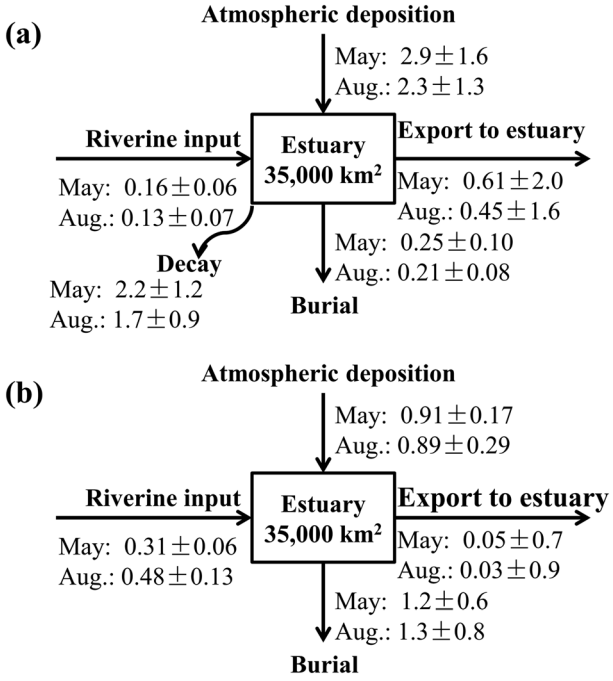

Figure 6. Budget (10^{12} Bq/month) of (a) ^{7}Be and (b) ^{210}Pb in the estuary region of the ECS.

$$(S_1 \times R_1) + (S_2 \times R_2) = S_x \quad (1)$$

$$R_1 + R_2 = 1 \quad (2)$$

where S_1, S_2, and S_x represent the SIRM values of Changjiang input ($1{,}090 \times 10^{-5}$ Am^2/kg; Zhang et al., 2008), relict sand (274×10^{-5} Am^2/kg, the minimum value observed in station F2), and the regional sediments, respectively. The R_1 and R_2 are the proportional contribution of S_1 and S_2 to the regional SIRM values. The calculated results showed that the contributions from the Changjiang input to SIRM values in surface sediment of F in August were 13% at 8F4. Apparently, only a small fraction of riverine ferrimagnetic minerals can be transported to offshore (29°N, 123°E). It should be noted that such semiquantitation is an upper limit because in addition to the two end-members mixing other processes (e.g., mineral sorting) might also result in a decrease of SIRM value.

3.3. Radionucides as Tracers for Sediment Transport

3.3.1. Mass Balance of ^{7}Be and ^{210}Pb in the Estuary Region of the ECS

In the use of radionuclides as tracers for the assessment of sediment transport in estuary, coast, and shelf region, their source terms should be first assessed. In our earlier study we reported that the main sources of ^{7}Be and ^{210}Pb to the water and sediments in the ECS are atmospheric fallout, riverine input, and boundary scavenging (Du et al., 2016). The in situ production of ^{210}Pb from dissolved ^{226}Ra is negligible (Du et al., 2016; Huang et al., 2013). The sinks of ^{7}Be and ^{210}Pb in the ECS are removal onto suspended particulate matter and their subsequent sediment deposition and transport to areas adjoining the study area. For a typical residence time of three months of water in coastal areas of the ECS, the radioactive decay of ^{210}Pb is ~0.8% and which is negligible compared to the errors associated with the mass balance estimate. To use the ^{7}Be and ^{210}Pb as tracers for quantifying the cross-shelf transport of sediment in the Zhe-Min coast, the estuary-trapped flux of these nuclides need to be estimated. The boundary of the estuary and inner shelf of the ECS (i.e., estuary, 35,000 km^2 and inner shelf, 37,000 km^2; Figure 1) are defined by the particle size in sediments and mobile mud thickness (>1.0 cm; Su & Huh, 2002; Wang et al., 2016). Since this discussion pertains to the seasonal distribution of radionuclides, here we estimate the budget of ^{7}Be and ^{210}Pb over time scale of a month.

The atmospheric deposition and riverine input of ^{7}Be and ^{210}Pb during the previous two months prior to sampling is also expected to contribute to the sources of these radionuclides in the ECS (which is discussed blow). Therefore, we have used the mean value of three months. The mean atmospheric deposition fluxes of ^{7}Be and ^{210}Pb between March and May of 2011 in Shanghai were reported to be 83.7 ± 47.1 and 26.0 ± 4.7 Bq · m^{-2} · month^{-1}, respectively (31.3°N, 121.4°E) and those of ^{7}Be and ^{210}Pb between June and August of 2011 were reported to be 64.6 ± 35.0 and 25.6 ± 8.3 Bq · m^{-2} · month^{-1}, respectively (Du et al., 2015). Then the atmospheric deposition flux of ^{7}Be to the estuary was estimated to be $(2.9 \pm 1.6) \times 10^{12}$ Bq/month in May and $(2.3 \pm 1.3) \times 10^{12}$ Bq/month in August. The ^{210}Pb atmospheric depositional flux values in May and August were plotted in Figure 6. The riverine input of ^{7}Be and ^{210}Pb to the ECS is mainly from Changjiang input, and the contributions from other rivers are negligible as they only discharge 10% of freshwater to the ECS (Du et al., 2010, 2016). No data are reported for the Changjiang input of ^{7}Be and ^{210}Pb during 2011, and thus, we have used the data from 2010. The mean activity of total ^{7}Be and ^{210}Pb (particulate form + dissolved form) in Xuliujing, a gauge station in Changjiang mouth (31.8°N, 121.0°E), were reported to be 3.4 ± 1.2 and 6.8 ± 1.3 Bq/m^3 during March and May 2010, respectively, and those during June and August were reported to be 1.5 ± 0.8 and 5.8 ± 1.6 Bq/m^3, respectively (Du et al., 2016). Using the water discharge of Changjiang during May (17,000 m/s) and August (31,000 m/s) (Wang et al., 2016), we estimated the riverine input flux from Changjiang River and is given in Figure 6.

Beryllium-7 delivered by atmospheric deposition and Changjiang would undergo radioactive decay prior to its removal by absorption onto suspended particulate matter and its eventual deposition as sediment. Considering the mean residence time of ^{7}Be in the water column of the Changjiang Estuary varied and from less 1 to 55 days (Huang et al., 2013), and thus, we assume that the atmospheric fallout and riverine input during two months prior to the sampling time also contributed the ^{7}Be to the estuary region. The fraction of the total ^{7}Be undergoing radioactive decay during past three months is estimated to be 67%–71% (total supply: $(3.3 \pm 1.6) \times 10^{12}$ Bq/month in May and $(2.4 \pm 1.3) \times 10^{12}$ Bq/month, respectively, and removal from decay: $(2.2 \pm 1.2) \times 10^{12}$ Bq/month in May and $(1.7 \pm 0.9) \times 10^{12}$ Bq/month in August, respectively) for May and August, respectively. The annual sedimentary deposition of ^{7}Be and ^{210}Pb (Bq/year) and can be obtained from the following equation:

$$B_x = A_x \times \rho \times R \times S \tag{3}$$

where A_x is the mean activity of ^{7}Be and ^{210}Pb in surface sediment of estuary region (8.1 ± 1.9 and 7.0 ± 1.0 Bq/kg for ^{7}Be in May and August, respectively, and 38 ± 16 and 44 ± 24 Bq/kg for ^{210}Pb in May and August, respectively; Wang et al., 2016), ρ is mean bulk density of the surface sediment (700 kg m^{-3}; Jia et al., 2018), R is the mean sedimentation rate in estuary region (0.015 ± 0.005 m/year; Deng et al., 2006), and S is the total surface area (m^2) of the estuarine region. The amounts of ^{7}Be and ^{210}Pb buried in the sediments in May and August can be estimated as given in Figure 6. From the mass balance, we found that the dominant source of ^{7}Be in the estuary is atmospheric fallout (~95%) in both May and August and 18%–20% of the total ^{7}Be was transported out of the estuary in both May and August. Distribution of ^{7}Be inventory (Figure 7 in Wang et al., 2016) and ^{7}Be/^{210}Pb$_{ex}$ activity ratios (Figure 5) suggested that the exported ^{7}Be out of estuary were mainly transported northeastward in summer and southward in spring (more details in section 3.4). The atmospheric fallout also dominated the source of ^{210}Pb in the estuary in both May (74%) and August (65%). There was a small fraction of ^{210}Pb exported out this region, with a value of $(0.03–0.05) \times 10^{12}$ Bq/month, respectively. These values are small compared to other sinks and are associated with very large uncertainties, and thus, the ^{210}Pb exported from the estuary is negligible in this study area.

3.3.2. A Particle Transport Model for the Inner Shelf of the ECS

Our recent study showed that the residence time of mobile mud was estimated to be three to six years in the Zhe-Min coast (Wang et al., 2016), which implies that the mobile mud undergoing settling-resuspension-transport-setting cycles was in a year time scale prior to its eventually sedimentary burial and cross-shelf transport, and thus, here we use ^{210}Pb to trace the cross-shelf transport of sediment in this region. The inputs of ^{210}Pb to the water column in the inner shelf of the ECS (box) are atmospheric deposition (J_{atm}, Bq/year) and cross-front exchange ($V\Delta C_f$) from the middle shelf, while the outputs of ^{210}Pb from the box are the advective transport by coastal current $\left(T\left(\overline{C}_d - \overline{C}_u\right)\right)$, burial flux to bottom sediments (J_{sed}, Bq/year), and net export to the shelf by particle transport (J_{exp}, Bq/year). The ^{210}Pb balance can be written as follows (Bacon et al., 1994):

$$J_{atm} + V\Delta C_f = T\left(\overline{C}_d - \overline{C}_u\right) + J_{sed} + J_{exp} \tag{4}$$

where V and ΔC_f represent cross-front exchange rate (m^3/s) and cross-front ^{210}Pb concentration difference (Bq/m^3), respectively; T is mean water volume transport of coastal current, which was reported to be 0.215×10^6 m^3/s (Wu et al., 2013); and C_d and $\overline{C}_u$ are mean ^{210}Pb concentrations (Bq/m^3) before input to the box and after output of the box, respectively.

The atmospheric deposition flux of ^{210}Pb to the inner shelf of the ECS (between 26°N and 30°N) can be estimated by using the previously reported data for the coastal cities of this study area. As it has been discussed above, the sediments would resuspend, transport, and redeposit for three to six years prior to eventually burial in the Zhe-Min coast (Wang et al., 2016), and thus, a longer time scale of atmospheric deposition flux of ^{210}Pb is more representatively used to assess the contribution of atmospheric deposition compared to a one-year time of measured values. Direct measurements over eight-year period at Shanghai yielded a mean flux of 366 Bq · m^{-2} · year (Du et al., 2015). Then the atmospheric deposition ^{210}Pb to the inner shelf of the ECS was estimated to be 14×10^{12} Bq/year. As mentioned above, the cross-front exchange would contribute a fraction of ^{210}Pb in to the model-box. The ΔC_f values of three sections (i.e., D, E, and F) from middle shelf to inner shelf in May of 2013 were 0.05, 0.12, and 0.32 Bq/m^3, and we take a mean value of 0.16 ± 0.14 Bq/m^3 to estimate the cross-front exchange ^{210}Pb flux. From the climatological simulations of

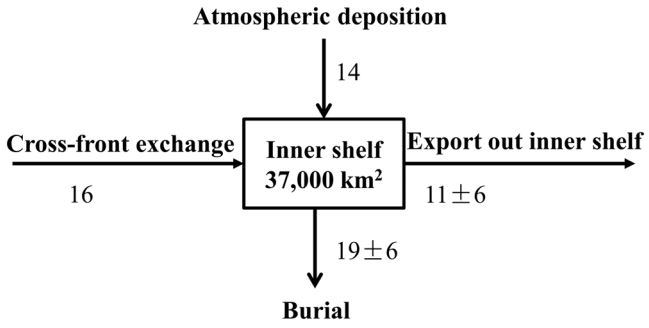

Figure 7. ^{210}Pb budget (10^{12} Bq/year) in the inner shelf of the ECS. The values of cross-front exchange and net export of inner shelf were upper limit, and thus, the uncertainties of these two items are not given.

Zhou et al. (2015), the annual mean volume of water transported across the shelf (0–100 m) is inward and reported to be 1.65×10^6 m^3/s. From these values, a net flux of ^{210}Pb ($V\Delta C_f$) spread over inner shelf resulted in a flux of $(8.3 \pm 7.3) \times 10^{12}$ Bq/year. Here we adopted a maximum value of 16×10^{12} Bq/year for estimating the upper limit value of J_{exp}.

As has been discussed above, the total ^{210}Pb concentration in seawater of the box varied a little and the mean ^{210}Pb concentrations of $\overline{C}_d$ and $\overline{C}_u$ were estimated to be 1.71 ± 0.29 Bq/m^3 (n = 6) and 1.47 ± 0.27 Bq/m^3 (n = 5), respectively (Su, 2015), which gives a difference of 0.24 ± 0.40 Bq/m^3. Using this value and the advective water volume 0.215×10^6 m^3/s, we can get a mean ^{210}Pb flux of $(1.6 \pm 2.7) \times 10^{12}$ Bq/year across the inner shelf of the ECS. This value is clearly smaller than the total value of the atmospheric deposition flux and cross-front exchange flux (~5%) and is associated with very large uncertainties, and thus, the removal by the advective transport is negligible for the box. The burial flux to sediments can be estimated to be $(19 \pm 6) \times 10^{12}$ Bq/year by using equation (3), mean sedimentation rate (0.008 ± 0.002 m/year; Deng et al., 2006), bulk density (700 g/m^3; Jia et al., 2018), and the surface area of the inner shelf of the ECS (37,000 km^2). Then the net export of ^{210}Pb was estimated to be $(11 \pm 6) \times 10^{12}$ Bq/year by using other input and output items (Figure 7). Though a net export ^{210}Pb was obtained, the mass balance estimation produced large uncertainties, which should result from the spatial variation of the sedimentation rate, ^{210}Pb concentration in surface sediments and seawater, and the complex hydrographic and topographical settings in the ECS.

Then we can determine export of particle mass ($J_{exp,p}$, g/year) by measuring the ratios of suspended particulate matter concentration to the content of ^{210}Pb (Bacon et al., 1994):

$$J_{exp,p} = J_{exp} \times C_p / C_{Pb}. \quad (5)$$

where C_p/C_{Pb} is the mean ratio (g/Bq) of suspended particulate matter concentration (g/L) and the concentration of ^{210}Pb (Bq/L) in the particulate matter. This mean ratio was reported to be 2.7 g/Bq in the same region (Su, 2015). Here we use a simple model applicable to only refractory suspended matter, and only considered just the physical transport of the particles, ignoring particle production and consumption (Bacon et al., 1994). Then the net export particle from the box was estimated to be $(2.8 \pm 1.5) \times 10^7$ ton/year using equation (5). This upper estimated value is only ~14% of annual sediment discharge (~2×10^8 ton/year) of Changjiang to the ECS and comparable to the magnetic parameter-based value of (13%) at station 8F4. Such a small value (14%) is similar to the previous estimation (15%) in the continental shelf of Middle Atlantic Bight (Bacon et al., 1994).

3.4. Comparison of Radionuclides and Magnetic Tracers

Both ^{7}Be and ^{210}Pb have similar sources (i.e., direct atmospheric deposition and riverine input) in the estuary region, and thus, ^{7}Be/^{210}Pb$_{ex}$ ratios are expected to be higher in the estuary followed by gradual decrease with distance away from the river mouth (Du et al., 2016; Saari et al., 2010). As a result, ^{7}Be/^{210}Pb$_{ex}$ ratios can be used to assess the seasonal transport of sediment from land to ocean. Because most of the ^{234}Th in marine environments is produced by the decay of dissolved ^{238}U, particulate ^{234}Th is commonly utilized to evaluate oceanic particulate cycling, sediment focusing, and lateral input of particulate matter (Du et al., 2016; Wang et al., 2016); the ^{234}Th$_{ex}$/^{210}Pb$_{ex}$ activity ratio in sediments could reduce the effect of particle sizes and mineral components and better reflect the oceanic processes. In summer, the ^{7}Be/^{210}Pb$_{ex}$ ratio decreased from the Changjiang Estuary to the northeast (Figure 5e), indicating transport of riverine sediments northeastward. In May, this ratio generally decreased from the estuary to the south along the Zhe-Min coast (from C0 to E1), thus suggesting that the sediment followed a southward transport pathway in spring (Figure 5b). Du et al. (2016) also found similar trend, and the ^{7}Be/^{210}Pb$_{ex}$ activity ratios of surface sediments in southern region of Changjiang Estuary were much higher during June 2010 compared to that in November 2010. These observations agree with our mass balance estimation that a higher fraction of ^{7}Be, compared to ^{210}Pb$_{ex}$, was transported out of the estuary in both May and August. This is attributed to lower K_d of ^{7}Be compared to ^{210}Pb, as ~90% of ^{7}Be and ^{210}Pb exist in dissolved phase in coastal and shelf regions

(Baskaran & Santschi, 1993). The distribution of $^{7}Be/^{210}Pb_{ex}$ activity ratios indicates that part of ^{7}Be mainly was transported southward in May and northeastward in August. This corresponds to the seasonal variations in suspended sediment transport driven by the CDW (Chen et al., 2006), which flows northeastward in summer and southward in spring and winter. Such seasonal variations in ^{7}Be inventories were also reported in the Mississippi River deltaic region (Corbett et al., 2004).

In contrast to the $^{7}Be/^{210}Pb_{ex}$ ratio, the χ_{ARM}/SIRM ratio indicated the occurrence of cross-shelf transport of sediments, which includes the southeast offshore transport (section C) in May, as well as offshore delivery along the Zhe-Min coast during both seasons (Figures 5a and 5d). Such a cross-shelf pathway of particulate matter has been reported in previous hydrodynamic and geochemical studies. For example, some studies have suggested that cross-shelf delivery occurs in section C (from 31.2°N, 123.1°E to 28.7°N, 127.1°E; Hoshika et al., 2003; Iseki et al., 2003). Zhu et al. (2011) reported that between 28°N and 29°N, sedimentary organic carbon in surface sediments was transported offshore (to 124°E); this observation was subsequently confirmed by physical oceanography studies (Wu, 2015; Yuan et al., 2005). The mechanism of such cross-shelf transport is complex, and according to previous studies the offshore transport in section C is via near-bottom sediment transport controlled by the downwelling and seaward bottom flow in inner shelf of the ECS (Hoshika et al., 2003). In the Zhe-Min coast (28–29°N), the suspended sediments might be transported offshore by the processes called penetrating front that occurs in the upper 20 m (Wu, 2015; Yuan et al., 2005). Wu (2015) suggested that such a cross-shelf transport is due to the ambient pycnocline undulation caused by tidal wave divergence. Near the bottom, the tidal pumping (Deng et al., 2017) and offshore bottom Ekman transport under the downwelling-favorable wind and coastal current (Liu et al., 2006; Wu, 2015) might also be important. The ^{210}Pb budget- and SIRM-based estimated results in the inner shelf of the ECS yielded a quantitative estimate for the cross-shelf sediment transport, accounting for 13%–14% of annual Changjiang sediment discharge. The differences in the results obtained using $^{7}Be/^{210}Pb_{ex}$ ratio; the χ_{ARM}/SIRM ratio is likely related to the differences in the behavior of magnetic minerals and radionuclides and life times as well as source terms of ^{7}Be, which is discussed below.

3.5. Factors Influencing Radionuclide and Magnetic Tracers

Although ^{7}Be, ^{234}Th, and ^{210}Pb are particle-reactive nuclides, the activities of these nuclides were observed to exhibit weak linear correlations with the clay fraction in this study (Figure 8), indicating variable affinity of these nuclides to the clay mineral fraction. The correlation coefficients between magnetic parameter and activities of radionuclides are given in Table S2. The linear correlations between radionuclide activities and χ_{ARM}/SIRM ratios are relatively better than those between the radionuclide activities and the clay fraction. The stronger relationship between radionuclides and the χ_{ARM}/SIRM ratio may reflect the fact that fine-grained iron oxides are good carriers of radionuclides. Previous laboratory studies have also suggested that Pb and Th can be strongly adsorbed onto magnetic minerals (e.g., hematite and magnetite; Murphy et al., 1999; Rajput et al., 2016). The relationship between excess ^{210}Pb ($^{210}Pb_{ex}$), excess ^{234}Th ($^{234}Th_{ex}$), and the χ_{ARM}/SIRM ratio exhibited no regional differences because $^{234}Th_{ex}$ and $^{210}Pb_{ex}$ have stronger affinities for lithogenic particles and are less affected by organic matter in comparison to other radionuclides (e.g., ^{7}Be; Geibert & Usbeck, 2004; Yang et al., 2015). However, the relationship between ^{7}Be and the χ_{ARM}/SIRM ratio differed between the southern and northern regions of the study area (Figure 8). The transfer of atmospheric ^{7}Be to sediments can be influenced by organic matter or lithogenic particles (Yang et al., 2015). The sediment in the northern region of the study area is dominated by relatively higher fraction of coarser particles with lower clay fractions (~15%). Thus, these coarser particles showed a less efficient scavenging for ^{7}Be in this region. However, sediments in the southern region of the study area mainly composed of detrital particulate matter (with finer grain size), and their ^{7}Be contents exhibited significant positive correlation with the χ_{ARM}/SIRM ratio.

In addition to particle size and mineralogy of sediment, sediment age has also been reported to significantly affect the activities of radionuclides (Singleton et al., 2017). The *age* of sediment (t) can be estimated based on $^{7}Be/^{210}Pb_{ex}$ activity ratios using the following equation (modified from Matisoff et al., 2005):

$$t = 1/(\lambda_1 - \lambda_2) \times \left(\ln (A_1/A_2)_0 - \ln (A_1/A_2) \right) \quad (6)$$

where λ_1 and λ_2 are the decay constants of ^{7}Be and ^{210}Pb, respectively; (A_1/A_2) is the measured $^{7}Be/^{210}Pb_{ex}$ activity ratio of the sediment; and $(A_1/A_2)_0$ is the $^{7}Be/^{210}Pb$ activity ratio of initial site delivered to the

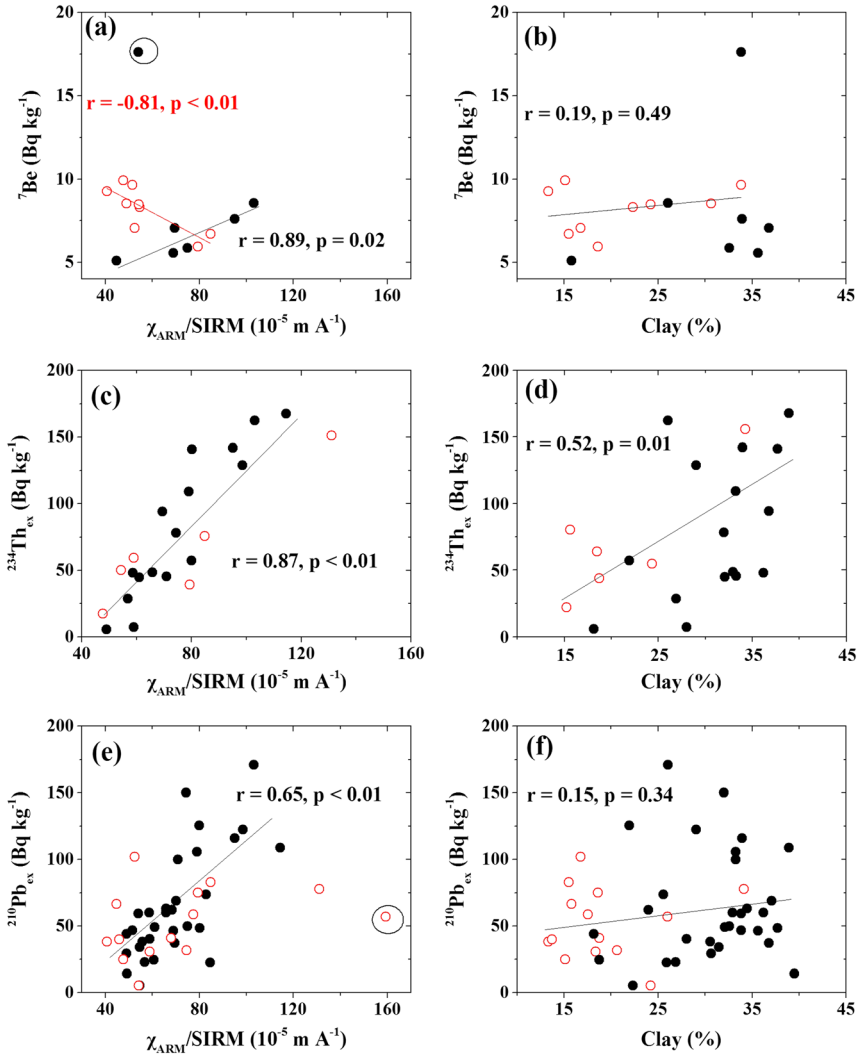

Figure 8. The relationships between radionuclides, χ_{ARM}/SIRM values, and clay. The red circle represents unit A, and the black dot represents unit B. The relationships between ^{7}Be activities and χ_{ARM}/SIRM ratios were separately analyzed for units A and B and others excluded figure (a) were analyzed together. The sites that were circled were not included for the correlation analyses.

sampling site. In this age estimate, it is assumed that once sedimentary particles are tagged with this $(A_1/A_2)_0$ ratio, this ratio changes only due to radioactive decay, and the tagged particles remain in a closed system. Although Matisoff et al. (2005) only considered contributions to $(A_1/A_2)_0$ from atmospheric input, in river-dominated settings, riverine input could also contribute a considerable proportion to the budgets of radionuclides. Thus, here we modified $(A_1/A_2)_0$ to represent the ^{7}Be/^{210}Pb activity ratio contributed from both direct atmospheric deposition and riverine contribution. From the mass balance of ^{7}Be and ^{210}Pb in the estuary region, the total of ^{7}Be from riverine and atmospheric input are estimated to be 3.1×10^{12} and 2.4×10^{12} Bq/month during May and August, respectively, and those of ^{210}Pb are estimated to be 1.2×10^{12} and 1.4×10^{12} Bq/month, respectively. Thus, the input ^{7}Be/^{210}Pb activity ratio can be calculated to be 2.6 and 1.7 during May and August, respectively, based on the total flux of atmospheric deposition and input from the Changjiang Estuary. Using equation (4), we can estimate the age of surface sediments near the estuary to be 10–42 days. For the age to be reliable, the new sediments in the estuary are expected to be mainly transported from the riverine particles and less from locally *older* particles. In the Zhe-Min coast, however, the mass balance of ^{210}Pb and our previous work indicated that the offshore input via *boundary scavenging* dominated the sources of ^{234}Th and ^{210}Pb to the coastal areas (Du et al., 2016; Wang et al., 2016). Thus, we could not directly use equation (1) to evaluate the age of sediment in

the Zhe-Min coast. The ^{7}Be activities below detection limit in offshore sediments were likely caused by the longer residence time of ^{7}Be in offshore water column (with maximum value of 140 days; Huang et al., 2013) or from the dilution by *older particles* from offshore. From our estimation presented above, more than half of ^{210}Pb in this region was transported from the outer shelf via boundary scavenging or upwelling (Figure 6). Therefore, ^{7}Be/^{210}Pb$_{ex}$ activity ratios failed to trace the transport of these terrigenous sediments to offshore in the Zhe-Min coast.

In the Changjiang Estuary, the sedimentation rates based on ^{7}Be were estimated to be ~4 cm/month, whereas those based on ^{210}Pb$_{ex}$ were 1–5 cm/year in the depocenter (McKee et al., 1983). This difference suggests that the Changjiang-derived sediments are resuspended on a seasonal basis and transported farther offshore, which corresponds to the southward longshore transport of sediment as indicated by ^{7}Be/^{210}Pb$_{ex}$, χ_{ARM}/SIRM ratios and in situ measurement using ADCP (Deng et al., 2017). It should be noted that lower ^{7}Be/^{210}Pb$_{ex}$ ratios were also observed on the southward longshore pathway of sediment transport in May (i.e., station D1). This was probably caused by the dilution of older resuspended sediments, which was likely caused by the upwelling current in this region (Liu et al., 2006). The higher ^{234}Th$_{ex}$/^{210}Pb$_{ex}$ ratios observed at this station suggested that an additional input of particles with ^{234}Th$_{ex}$ or dilution of ^{210}Pb$_{ex}$-laden fine particulate matter from the resuspension of bottom sediments (Figure 5b). These observations suggested that fresh river-loaded sedimentary particles were mixed with resuspended particles during their transportation southward in May. The older sediments, which were driven from resuspension by strong hydrodynamic conditions or strong winds, would have diluted the signal of ^{7}Be in these regions where strong resuspension occurred; thus, tracing riverine sediment transport is problematic in regions such as the Mississippi and Amazon deltas (Allison et al., 2005). For magnetic properties, postdepositional degradation of organic carbon might affect magnetic properties (Roberts, 2015); thus, in these settings the effect of diagenetic conditions should be considered when magnetic properties are utilized to indicate sediment transport. However, the impact of organic carbon degradation on magnetic properties in mobile mud in the river-dominated margin was relatively small due to the dominance of refractory organic matter, abundant iron oxides, and rapid accumulation rate (Ge et al., 2015; Roberts, 2015).

3.6. Implications of the Combined Radionuclide and Magnetic Tracing Methods

As discussed above, both our results based on magnetic properties and ^{210}Pb budget and other studies (e.g., Wu, 2015; Zhu et al., 2011) did not support the viewpoint that the salty and warm TWC completely blocked the cross-shelf transport of sedimentary particles to the middle shelf (e.g., Liu et al., 2007). Our results showed that sediments derived from cross-shelf transport in the Zhe-Min coast are only a small fraction of fine particles. The ^{7}Be/^{210}Pb$_{ex}$ can be used to indicate that the seasonal sediment transport pathway and ^{210}Pb budget associated with a particle transport model are useful to quantify the long-term (years to decades) cross-shelf transport of refractory suspended matter. Overall, radionuclides are preferable compared to magnetic properties for determining timescales of sediment dynamics (Allison et al., 2005; Saari et al., 2010; Sommerfield et al., 1999). Unlike radionuclides, χ_{ARM}/SIRM ratios reflect the internal properties of sedimentary minerals and can thus offer more detailed information on sediment transport directions or sorting dynamics. Although each method has been used to study sediment transport in river-dominated areas, such as the Amazon delta, the Gulf of Mexico, and the ECS (Ellwood et al., 2006; Liu et al., 2010; Rowan et al., 2009; Smoak et al., 1996), their combined use is rare. Once the boundary conditions on the regions of interest are constrained, from the measured radionuclides and ferrimagnetic minerals data we can obtain semiquantitative indications of sediment transport. Considering the nondestructive features of magnetic and radionuclide analyses, we suggest that a combined approach of particle-reactive radionuclides and magnetic properties in evaluating the temporal and spatial transport of sedimentary materials in river-dominated estuaries and coastal regions.

4. Conclusions

In the ECS, which is a river-dominated marginal sea in Pacific Ocean, seasonal sediment transport was examined using magnetic parameters and radionuclides (i.e., ^{7}Be, ^{234}Th$_{ex}$, and ^{210}Pb$_{ex}$). From the mass balance of ^{7}Be, we estimate that 18% of the total ^{7}Be in the estuary is exported southward in May and northeastward in August. This seasonal transport of sedimentary particulate matter agrees with the χ_{ARM}/SIRM-based results. Both ^{210}Pb budget and SIRM distribution in the inner shelf of the ECS showed

that a small fraction of fine particles could be transported out of inner shelf (70 m isobaths), which at most accounted for 14% of annual Changjiang sediment discharge. Most of ^{7}Be activities in inner shelf sediments of the ECS were below detection limit due to relatively lower residence times of ^{7}Be and dilution by the older sediment. Resuspension of bottom sediments with higher $^{210}Pb_{xs}$ activities as well as abundant of ^{210}Pb (>50%) transported from the outer shelf via boundary scavenging could explain this observation. The fact that radionuclides showed better correlation with the χ_{ARM}/SIRM ratio than with grain size suggests that magnetic minerals (i.e., iron oxides) are the primary carriers of particle-reactive radionuclides. The absorption of radionuclides onto magnetic minerals reinforces the reliability of the combined application of two methods. Our study suggests that radionuclides are preferable for determining timescales of sediment dynamics, whereas magnetic property data can offer more detailed information about sediment transport directions or sorting dynamics. The combined analysis of magnetic parameters and radionuclides yields a better understanding of sediment dynamics in river-dominated margins.

Acknowledgments

Original data on the thickness, water content, grain size, and activities of radionuclides in these surface sediments and sampling locations were reported in the Table 1 and Table S1 of our previous study (Wang et al., 2016). The measured values of magnetic parameters were listed in Table S1 of this paper. This research was supported by the Ministry of Science and Technology of the People's Republic of China (2011CB409801) and the National Natural Science Foundation of China (41706089 and 41576094). We thank Bing Deng for constructive discussion. We also wish to thank Editor, S. Bradley Moran and two anonymous reviewers for their constructive comments.

References

Aller, R. C. (1998). Mobile deltaic and continental shelf muds as suboxic, fluidized bed reactors. *Marine Chemistry*, *61*(3–4), 143–155. https://doi.org/10.1016/S0304-4203(98)00024-3

Aller, R. C., Heilbrun, C., Panzeca, C., Zhu, Z., & Baltzer, F. (2004). Coupling between sedimentary dynamics, early diagenetic processes, and biogeochemical cycling in the Amazon–Guianas mobile mud belt: Coastal French Guiana. *Marine Geology*, *208*(2–4), 331–360. https://doi.org/10.1016/j.margeo.2004.04.027

Allison, M. A., Sheremet, A., Goñi, M. A., & Stone, G. W. (2005). Storm layer deposition on the Mississippi–Atchafalaya subaqueous delta generated by Hurricane Lili in 2002. *Continental Shelf Research*, *25*(18), 2213–2232. https://doi.org/10.1016/j.csr.2005.08.023

Bacon, M. P., Belastock, R. A., & Bothner, M. H. (1994). ^{210}Pb balance and implications for particle transport on the continental shelf, US Middle Atlantic Bight. *Deep Sea Research Part II: Topical Studies in Oceanography*, *41*(2–3), 511–535. https://doi.org/10.1016/0967-0645(94)90033-7

Baskaran, M., & Santschi, P. H. (1993). The role of particles and colloids in the transport of radionuclides in coastal environments of Texas. *Marine Chemistry*, *43*(1–4), 95–114. https://doi.org/10.1016/0304-4203(93)90218-D

Baskaran, M., & Santschi, P. H. (2002). Particulate and dissolved ^{210}Pb activities in the shelf and slope regions of the Gulf of Mexico waters. *Continental Shelf Research*, *22*(10), 1493–1510. https://doi.org/10.1016/S0278-4343(02)00017-1

Baskaran, M., Santschi, P. H., Guo, L., Bianchi, T. S., & Lambert, C. (1996). ^{234}Th: ^{238}U disequilibria in the Gulf of Mexico: The importance of organic matter and particle concentration. *Continental Shelf Research*, *16*(3), 353–380. https://doi.org/10.1016/0278-4343(95)00016-T

Bianchi, T. S. (2011). The role of terrestrially derived organic carbon in the coastal ocean: A changing paradigm and the priming effect. *Proceedings of the National Academy of Sciences*, *108*(49), 19,473–19,481. https://doi.org/10.1073/pnas.1017982108

Blair, N. E., & Aller, R. C. (2012). The fate of terrestrial organic carbon in the marine environment. *Annual Review of Marine Science*, *4*(1), 401–423. https://doi.org/10.1146/annurev-marine-120709-142717

Bloemendal, J., & Liu, X. (2005). Rock magnetism and geochemistry of two Plio–Pleistocene Chinese loess–palaeosol sequences—Implications for quantitative palaeoprecipitation reconstruction. *Palaeogeography, Palaeoclimatology, Palaeoecology*, *226*(1–2), 149–166. https://doi.org/10.1016/j.palaeo.2005.05.008

Chen, S. L., Zhang, G. A., Yang, S. L., & Shi, J. Z. (2006). Temporal variations of fine suspended sediment concentration in the Changjiang River estuary and adjacent coastal waters, China. *Journal of Hydrology*, *331*(1–2), 137–145. https://doi.org/10.1016/j.jhydrol.2006.05.013

Corbett, D. R., McKee, B., & Duncan, D. (2004). An evaluation of mobile mud dynamics in the Mississippi River deltaic region. *Marine Geology*, *209*(1–4), 91–112. https://doi.org/10.1016/j.margeo.2004.05.028

Dai, Z., Liu, J. T., Wei, W., & Chen, J. (2014). Detection of the Three Gorges Dam influence on the Changjiang (Yangtze River) submerged delta. *Scientific Reports*, *4*(1), 6600. https://doi.org/10.1038/srep06600

Deng, B., Wu, H., Yang, S., & Zhang, J. (2017). Longshore suspended sediment transport and its implications for submarine erosion off the Yangtze River Estuary. *Estuarine, Coastal and Shelf Science*, *190*, 1–10. https://doi.org/10.1016/j.ecss.2017.03.015

Deng, B., Zhang, J., & Wu, Y. (2006). Recent sediment accumulation and carbon burial in the East China Sea. *Global Biogeochemical Cycles*, *20*, GB3014. https://doi.org/10.1029/2005GB002559

Dong, C., Zhang, W., He, Q., Dong, Y., & Yu, L. (2014). Magnetic fingerprinting of hydrodynamic variations and channel erosion across the turbidity maximum zone of the Yangtze Estuary, China. *Geomorphology*, *226*, 300–311. https://doi.org/10.1016/j.geomorph.2014.08.008

Du, J., Wu, Y., Huang, D., & Zhang, J. (2010). Use of ^{7}Be, ^{210}Pb and ^{137}Cs tracers to the transport of surface sediments of the Changjiang Estuary, China. *Journal of Marine Systems*, *82*(4), 286–294.

Du, J., Du, J., Baskaran, M., Bi, Q., Huang, D., & Jiang, Y. (2015). Temporal variations of atmospheric depositional fluxes of ^{7}Be and ^{210}Pb over 8 years (2006–2013) at Shanghai, China, and synthesis of global fallout data. *Journal of Geophysical Research: Atmospheres*, *120*, 4323–4339. https://doi.org/10.1002/2014JD022807

Du, J., Du, J., Huang, D., Wang, J., & Zhang, J. (2016). Seasonal distribution patterns of ^{7}Be and ^{210}Pb in surface sediments in the Changjiang Estuary, China and their implication. *Journal of Marine Systems*, *154*, 41–49. https://doi.org/10.1016/j.jmarsys.2015.05.001

Ellwood, B. B., Balsam, W. L., & Roberts, H. H. (2006). Gulf of Mexico sediment sources and sediment transport trends from magnetic susceptibility measurements of surface samples. *Marine Geology*, *230*(3–4), 237–248. https://doi.org/10.1016/j.margeo.2006.05.008

Evans, M., & Heller, F. (2003). *Environmental magnetism: Principles and applications of environmagnetics* (pp. 1–299). San Diego: Academic Press.

Feng, H., Cochran, J. K., & Hirschberg, D. J. (1999). ^{234}Th and ^{7}Be as tracers for the transport and dynamics of suspended particles in a partially mixed estuary. *Geochimica et Cosmochimica Acta*, *63*(17), 2487–2505. https://doi.org/10.1016/S0016-7037(99)00060-5

Ge, C., Zhang, W., Dong, C., Dong, Y., Bai, X., Liu, J., et al. (2015). Magnetic mineral diagenesis in the river-dominated inner shelf of the East China Sea, China. *Journal of Geophysical Research: Solid Earth*, *120*, 4720–4733. https://doi.org/10.1002/2015JB011952

Geibert, W., & Usbeck, R. (2004). Adsorption of thorium and protactinium onto different particle types: Experimental findings 1. *Geochimica et Cosmochimica Acta*, *68*(7), 1489–1501. https://doi.org/10.1016/j.gca.2003.10.011

Giffin, D., & Corbett, D. R. (2003). Evaluation of sediment dynamics in coastal systems via short-lived radioisotopes. *Journal of Marine Systems*, *42*(3–4), 83–96. https://doi.org/10.1016/S0924-7963(03)00068-X

Hatfield, R. G., Cioppa, M. T., & Trenhaile, A. S. (2010). Sediment sorting and beach erosion along a coastal foreland: Magnetic measurements in Point Pelee National Park, Ontario, Canada. *Sedimentary Geology*, *231*(3–4), 63–73. https://doi.org/10.1016/j.sedgeo.2010.09.007

Hoitink, A. J. F., Wang, Z. B., Vermeulen, B., Huismans, Y., & Kästner, K. (2017). Tidal controls on river delta morphology. *Nature Geoscience*, *10*(9), 637–645. https://doi.org/10.1038/ngeo3000

Horng, C. S., & Huh, C. A. (2011). Magnetic properties as tracers for source-to-sink dispersal of sediments: A case study in the Taiwan Strait. *Earth and Planetary Science Letters*, *309*(1–2), 141–152.

Hoshika, A., Tanimoto, T., Mishima, Y., Iseki, K., & Okamura, K. (2003). Variation of turbidity and particle transport in the bottom layer of the East China Sea. *Deep Sea Research Part II: Topical Studies in Oceanography*, *50*(2), 443–455. https://doi.org/10.1016/S0967-0645(02)00462-9

Huang, D., Du, J., Moore, W. S., & Zhang, J. (2013). Particle dynamics of the Changjiang Estuary and adjacent coastal region determined by natural particle-reactive radionuclides (^{7}Be, ^{210}Pb, and ^{234}Th). *Journal of Geophysical Research: Oceans*, *118*, 1736–1748. https://doi.org/10.1002/jgrc.20148

Iseki, K., Okamura, K., & Kiyomoto, Y. (2003). Seasonality and composition of downward particulate fluxes at the continental shelf and Okinawa Trough in the East China Sea. *Deep Sea Research Part II: Topical Studies in Oceanography*, *50*(2), 457–473. https://doi.org/10.1016/S0967-0645(02)00468-X

Jia, J., Gao, J., Cai, T., Li, Y., Yang, Y., Wang, Y. P., et al. (2018). Sediment accumulation and retention of the Changjiang (Yangtze River) subaqueous delta and its distal muds over the last century. *Marine Geology*, *401*, 2–16. https://doi.org/10.1016/j.margeo.2018.04.005

Kim, W., Doh, S. J., Yu, Y., & Lee, Y. I. (2013). Magnetic evaluation of sediment provenance in the northern East China Sea using fuzzy c-means cluster analysis. *Marine Geology*, *337*, 9–19. https://doi.org/10.1016/j.margeo.2013.01.001

Kruiver, P. P., Dekkers, M. J., & Heslop, D. (2001). Quantification of magnetic coercivity components by the analysis of acquisition curves of isothermal remanent magnetisation. *Earth and Planetary Science Letters*, *189*(3–4), 269–276. https://doi.org/10.1016/S0012-821X(01)00367-3

Laceby, J. P., Evrard, O., Smith, H. G., Blake, W. H., Olley, J. M., Minella, J. P., & Owens, P. N. (2017). The challenges and opportunities of addressing particle size effects in sediment source fingerprinting: A review. *Earth-Science Reviews*, *169*, 85–103. https://doi.org/10.1016/j.earscirev.2017.04.009

Li, W., Hu, Z., Zhang, W., Ji, R., & Nguyen, T. T. H. (2017). Influence of provenance and hydrodynamic sorting on the magnetic properties and geochemistry of sediments of the Oujiang River, China. *Marine Geology*, *387*, 1–11. https://doi.org/10.1016/j.margeo.2017.03.002

Lin, S., Hsieh, I. J., Huang, K. M., & Wang, C. H. (2002). Influence of the Yangtze River and grain size on the spatial variations of heavy metals and organic carbon in the East China Sea continental shelf sediments. *Chemical Geology*, *182*(2–4), 377–394. https://doi.org/10.1016/S0009-2541(01)00331-X

Liu, J. P., Li, A. C., Xu, K. H., Velozzi, D. M., Yang, Z. S., Milliman, J. D., & DeMaster, D. J. (2006). Sedimentary features of the Yangtze River-derived along-shelf clinoform deposit in the East China Sea. *Continental Shelf Research*, *26*(17–18), 2141–2156. https://doi.org/10.1016/j.csr.2006.07.013

Liu, J. P., Xu, K. H., Li, A. E. A., Milliman, J. D., Velozzi, D. M., Xiao, S. B., & Yang, Z. S. (2007). Flux and fate of Yangtze River sediment delivered to the East China Sea. *Geomorphology*, *85*(3–4), 208–224. https://doi.org/10.1016/j.geomorph.2006.03.023

Liu, S., Zhang, W., He, Q., Li, D., Liu, H., & Yu, L. (2010). Magnetic properties of East China Sea shelf sediments off the Yangtze Estuary: Influence of provenance and particle size. *Geomorphology*, *119*(3–4), 212–220. https://doi.org/10.1016/j.geomorph.2010.03.027

Maher, B. A. (1988). Magnetic properties of some synthetic sub-micron magnetites. *Geophysical Journal International*, *94*(1), 83–96. https://doi.org/10.1111/j.1365-246X.1988.tb03429.x

Matisoff, G., Wilson, C. G., & Whiting, P. J. (2005). The ^{7}Be/^{210}Pb$_{xs}$ ratio as an indicator of suspended sediment age or fraction new sediment in suspension. *Earth Surface Processes and Landforms*, *30*(9), 1191–1201. https://doi.org/10.1002/esp.1270

McKee, B. A., Aller, R. C., Allison, M. A., Bianchi, T. S., & Kineke, G. C. (2004). Transport and transformation of dissolved and particulate materials on continental margins influenced by major rivers: Benthic boundary layer and seabed processes. *Continental Shelf Research*, *24*(7–8), 899–926. https://doi.org/10.1016/j.csr.2004.02.009

McKee, B. A., Nittrouer, C. A., & DeMaster, D. J. (1983). Concepts of sediment deposition and accumulation applied to the continental shelf near the mouth of the Yangtze River. *Geology*, *11*(11), 631–633. https://doi.org/10.1130/0091-7613(1983)11<631:COSDAA>2.0.CO;2

Milliman, J. D., Shen, H. T., Yang, Z. S., & Robert, H. M. (1985). Transport and deposition of river sediment in the Changjiang Estuary and adjacent continental shelf. *Continental Shelf Research*, *4*(1–2), 37–45. https://doi.org/10.1016/0278-4343(85)90020-2

Murphy, R. J., Lenhart, J. J., & Honeyman, B. D. (1999). The sorption of thorium (IV) and uranium (VI) to hematite in the presence of natural organic matter. *Colloids and Surfaces A: Physicochemical and Engineering Aspects*, *157*(1–3), 47–62. https://doi.org/10.1016/S0927-7757(99)00115-6

Nguyen, T. T. H., Zhang, W., Li, Z., Li, J., Ge, C., Liu, J., et al. (2016). Magnetic properties of sediments of the Red River: Effect of sorting on the source-to-sink pathway and its implications for environmental reconstruction. *Geochemistry, Geophysics, Geosystems*, *17*, 270–281. https://doi.org/10.1002/2015GC006089

Palinkas, C. M., Nittrouer, C. A., Wheatcroft, R. A., & Langone, L. (2005). The use of ^{7}Be to identify event and seasonal sedimentation near the Po River delta, Adriatic Sea. *Marine Geology*, *222*, 95–112.

Rajput, S., Pittman, C. U. Jr., & Mohan, D. (2016). Magnetic magnetite (Fe_3O_4) nanoparticle synthesis and applications for lead (Pb^{2+}) and chromium (Cr^{6+}) removal from water. *Journal of Colloid and Interface Science*, *468*, 334–346. https://doi.org/10.1016/j.jcis.2015.12.008

Roberts, A. P. (2015). Magnetic mineral diagenesis. *Earth-Science Reviews*, *151*, 1–47. https://doi.org/10.1016/j.earscirev.2015.09.010

Rowan, C. J., Roberts, A. P., & Broadbent, T. (2009). Reductive diagenesis, magnetite dissolution, greigite growth and paleomagnetic smoothing in marine sediments: A new view. *Earth and Planetary Science Letters*, *277*(1–2), 223–235. https://doi.org/10.1016/j.epsl.2008.10.016

Saari, H. K., Schmidt, S., Castaing, P., Blanc, G., Sautour, B., Masson, O., & Cochran, J. K. (2010). The particulate ^{7}Be/^{210}Pb$_{xs}$ and ^{234}Th/^{210}Pb$_{xs}$ activity ratios as tracers for tidal-to-seasonal particle dynamics in the Gironde estuary (France): Implications for the budget of particle-associated contaminants. *Science of the Total Environment*, *408*(20), 4784–4794. https://doi.org/10.1016/j.scitotenv.2010.07.017

Shi, W., & Wang, M. (2010). Satellite observations of the seasonal sediment plume in central East China Sea. *Journal of Marine Systems*, *82*(4), 280–285. https://doi.org/10.1016/j.jmarsys.2010.06.002

Singleton, A. A., Schmidt, A. H., Bierman, P. R., Rood, D. H., Neilson, T. B., Greene, E. S., et al. (2017). Effects of grain size, mineralogy, and acid-extractable grain coatings on the distribution of the fallout radionuclides ^{7}Be, ^{10}Be, ^{137}Cs, and ^{210}Pb in river sediment. *Geochimica et Cosmochimica Acta*, *197*, 71–86. https://doi.org/10.1016/j.gca.2016.10.007

Smoak, J. M., DeMaster, D. J., Kuehl, S. A., Pope, R. H., & McKee, B. A. (1996). The behavior of particle-reactive tracers in a high turbidity environment: ^{234}Th and ^{210}Pb on the Amazon continental shelf. *Geochimica et Cosmochimica Acta*, *60*(12), 2123–2137. https://doi.org/10.1016/0016-7037(96)00092-0

Sommerfield, C. K., Nittrouer, C. A., & Alexander, C. R. (1999). ^{7}Be as a tracer of flood sedimentation on the northern California continental margin. *Continental Shelf Research*, *19*(3), 335–361. https://doi.org/10.1016/S0278-4343(98)00090-9

Su, C. C., & Huh, C. A. (2002). ^{210}Pb, ^{137}Cs and ^{239,240}Pu in East China Sea sediments: sources, pathways and budgets of sediments and radionuclides. *Marine Geology*, *183*(1–4), 163–178.

Su, J. L. (2001). A review of circulation dynamics of the coastal oceans near China (in Chinese). *Haiyang Xuebao*, *23*(4), 1–16.

Su, K. (2015). Seasonal change in the 210Po/210Pb disequilibrium and their implication of the export fluxes of particulate of organic carbon in upper layer water of the East China Sea. Master Dissertation. East China Normal University, China. pp. 1–106 (In Chinese with English abstract).

Syvitski, J. P., Kettner, A. J., Overeem, I., Hutton, E. W., Hannon, M. T., Brakenridge, G. R., et al. (2009). Sinking deltas due to human activities. *Nature Geoscience*, *2*(10), 681–686. https://doi.org/10.1038/ngeo629

Thompson, R., & Oldfield, F. (1986). *Environmental Magnetism* (pp. 1–227). London: Allen and Unwin. https://doi.org/10.1007/978-94-011-8036-8

Wang, J., Baskaran, M., Hou, X., Du, J., & Zhang, J. (2017). Historical changes in ^{239}Pu and ^{240}Pu sources in sedimentary records in the East China Sea: Implications for provenance and transportation. *Earth and Planetary Science Letters*, *466*, 32–42. https://doi.org/10.1016/j.epsl.2017.03.005

Wang, J., Du, J., Baskaran, M., & Zhang, J. (2016). Mobile mud dynamics in the East China Sea elucidated using ^{210}Pb, ^{137}Cs, ^{7}Be, and ^{234}Th as tracers. *Journal of Geophysical Research: Oceans*, *121*, 224–239. https://doi.org/10.1002/2015JC011300

Wei, W., Chang, Y., & Dai, Z. (2014). Streamflow changes of the Changjiang (Yangtze) River in the recent 60 years: Impacts of the East Asian summer monsoon, ENSO, and human activities. *Quaternary International*, *336*, 98–107. https://doi.org/10.1016/j.quaint.2013.10.064

Wu, H. (2015). Cross-shelf penetrating fronts: A response of buoyant coastal water to ambient pycnocline undulation. *Journal of Geophysical Research: Oceans*, *120*, 5101–5119. https://doi.org/10.1002/2014JC010686

Wu, H., Deng, B., Yuan, R., Hu, J., Gu, J., Shen, F., et al. (2013). Detiding measurement on transport of the Changjiang-derived buoyant coastal current. *Journal of Physical Oceanography*, *43*(11), 2388–2399. https://doi.org/10.1175/JPO-D-12-0158.1

Xing, F., Wang, Y. P., & Wang, H. V. (2012). Tidal hydrodynamics and fine-grained sediment transport on the radial sand ridge system in the southern Yellow Sea. *Marine Geology*, *291*, 192–210.

Yang, W., Guo, L., Chuang, C. Y., Santschi, P. H., Schumann, D., & Ayranov, M. (2015). Influence of organic matter on the adsorption of ^{210}Pb, ^{210}Po and ^{7}Be and their fractionation on nanoparticles in seawater. *Earth and Planetary Science Letters*, *423*, 193–201. https://doi.org/10.1016/j.epsl.2015.05.007

Yuan, D., Qiao, F., & Su, J. (2005). Cross-shelf penetrating fronts off the southeast coast of China observed by MODIS. *Geophysical Research Letters*, *32*, L19603. https://doi.org/10.1029/2005GL023815

Zhang, W., Ma, H., Ye, L., Dong, C., Yu, L., & Feng, H. (2012). Magnetic and geochemical evidence of Yellow and Yangtze River influence on tidal flat deposits in northern Jiangsu Plain, China. *Marine Geology*, *319*, 47–56.

Zhang, W., Xing, Y., Yu, L., Feng, H., & Lu, M. (2008). Distinguishing sediments from the Yangtze and Yellow Rivers, China: A mineral magnetic approach. *The Holocene*, *18*(7), 1139–1145. https://doi.org/10.1177/0959683608095582

Zhou, F., Xue, H., Huang, D., Xuan, J., Ni, X., Xiu, P., & Hao, Q. (2015). Cross-shelf exchange in the shelf of the East China Sea. *Journal of Geophysical Research: Oceans*, *120*, 1545–1572. https://doi.org/10.1002/2014JC010567

Zhou, L., Liu, J., Saito, Y., Zhang, Z., Chu, H., & Hu, G. (2014). Coastal erosion as a major sediment supplier to continental shelves: Example from the abandoned old Huanghe (Yellow River) delta. *Continental Shelf Research*, *82*, 43–59. https://doi.org/10.1016/j.csr.2014.03.015

Zhu, C., Wang, Z. H., Xue, B., Yu, P. S., Pan, J. M., Wagner, T., & Pancost, R. D. (2011). Characterizing the depositional settings for sedimentary organic matter distributions in the Lower Yangtze River-East China Sea Shelf System. *Estuarine, Coastal and Shelf Science*, *93*(3), 182–191. https://doi.org/10.1016/j.ecss.2010.08.001